ISSN 0022-4766, Journal of Structural Chemistry, 2022, Vol. 63, No. 6, pp. 885-894. © Pleiades Publishing, Ltd., 2022.
Russian Text © The Author(s), 2022, published in Zhurnal Strukturnoi Khimii, 2022, Vol. 63, No. 6, pp. 751-760.

OPERANDO X-RAY DIFFRACTION ANALYSIS OF THE MnO_x–ZrO_2 CATALYST DURING OXIDATION OF PROPANE

O. A. Bulavchenko[1]*, Z. S. Vinokurov[1,2], V. P. Konovalova[1], and T. N. Afonasenko[3]

A series of MnO_x–ZrO_2 catalysts is prepared by coprecipitation with variation of the calcinationtemperature from 400 °C to 800 °C. It is shown that the catalyst calcined at 650-700 °C exhibits the highest activity in the propane oxidation reaction. The MnO_x–ZrO_2 catalyst is studied by operando X-ray diffraction under conditions of the propane oxidation reaction. The structural features of the catalyst are examined upon heating in propane or oxygen media or at the propane:oxygen ratio of 1:6. It is found that in pure propane, there is the dehydrogenation reaction on the catalyst with the formation of propylene and hydrogen and is accompanied by a change in the catalyst structure. The initial catalyst consists of a (Mn, Zr)O_2 solid solution and Mn_2O_3 oxide. During the reaction, Mn cations are reduced in both (Mn, Zr)O_2 solid solution bulk and compositions of crystalline oxides: $Mn_2O_3 \rightarrow Mn_3O_4 \rightarrow MnO$. Under the catalytic conditions of the propane oxidation reaction and in pure oxygen, the catalyst structure remains unchanged.

DOI: 10.1134/S0022476622060051

Keywords: zirconium oxide, fluorite, powder X-ray diffraction, manganese oxide, in situ, “operando”.

INTRODUCTION

At present, many works have been published on the application of manganese-containing oxides as catalysts. Interest in catalysts based on transition metals is explained by their practical importance: they are an alternative to catalysts based on precious metals, combining a low cost, an increased thermal stability, and the resistance to poisoning with chlorine- and sulfur-containing compounds [1-3]. The activity of manganese oxides is due to the ability of ions of this element to easily change the oxidation state, the variety of its oxides, and the capacity of its crystal lattice with respect to oxygen. Manganese-containing oxides can also be used as catalysts for the oxidation of hydrocarbons and volatile organic compounds and in selective reduction reactions. In all the cases mentioned, the redox properties of manganese oxides play the key role. Moreover, it is must be kept in mind that the activity of these catalysts is directly associated with conditions of the process. For instance, the phase composition and charge state of oxides substantially change depending on the fuel combustion conditions (excess or deficiency of fuel (hydrogen, hydrocarbons) in the gas mixture.

[1]Boreskov Institute of Catalysis, Siberian Branch, Russian Academy of Sciences, Novosibirsk, Russia; *obulavchenko@catalysis.ru. [2]SKIF Center, Institute of Catalysis, Siberian Branch, Russian Academy of Sciences, Kol’tsovo, Russia. [3]Center of New Chemical Technologies, Institute of Catalysis, Siberian Branch, Russian Academy of Sciences, Omsk, Russia. Original article submitted October 7, 2021; revised December 31, 2021; accepted January 12, 2022.

In mixtures with a high content of fuel, manganese is mainly in Mn_3O_4 or MnO states; in mixtures depleted with fuel, oxygen-enriched MnO_x (Mn_2O_3 or MnO_2) particles are stabilized [4]. Stobbe et al. investigated manganese oxides as compounds stocking up oxygen during cyclic methane oxidation. Manganese oxides are reduced in methane to low-valent MnO oxide. In the oxygen-containing atmosphere, MnO particles rapidly transform into Mn_3O_4 and Mn_2O_3 [5]. Pike and coauthors performed in situ diffraction experiments to analyze the reduction of Mn_3O_4 to MnO in CO and reverse oxidation of MnO to Mn_3O_4, Mn_5O_8, Mn_2O_3 with oxygen [6]. The structure of manganese oxides is sensitive to the treatment medium, reduction and reverse reoxidation processes readily proceed, with the routes of solid-phase transformations depending on treatment conditions and the precursor structure.

According to a number of works, the cationic environment also significantly affects the oxide redox properties [7, 8]. The reduction of $(Mn,Co)_3O_4$ mixed oxides differs from the processes occurring in Mn_3O_4 and Co_3O_4 simple oxides, which is related to that there are two cations in one oxide matrix in which oxygen is more strongly held by the oxide structure [8-10]. $(Mn,Ga)_3O_4$ is characterized by the reduction of Mn cations in the solid solution bulk with a loss of excess oxygen at first, and then the isolation of MnO as a separate phase [7, 11]. For $(Mn, Zr)O_2$ mixed oxide it is shown that its reduction is a two-step process. At the first step, manganese cations ($Mn^{3+} \rightarrow Mn^{2+}$) are reduced in the solid solution bulk; at the second step, manganese cations are segregated on the surface. During further reoxidation, manganese remained on the surface as manganese oxide particles [12]. However, the behavior of the system remains unclear when oxidation and reduction processes compete with each, as it occurs during a catalytic reaction. The effect of the CO/O_2 ratio on the structure of the MnO_x–ZrO_2 catalyst with the cation ratio Mn/Zr = 3/2 has been studied previously: in an excess of CO, catalyst reduction was observed, however, this process is reversible, and reoxidation leads to the formation of the initial state [13]. If the reagent nature is varied, the processes taking place in the catalyst bulk can change because of different adsorption characteristics of substrates and the occurrence of additional reactions (formation of carbon on the catalyst surface, carbides in the interaction with hydrocarbons).

The aim of this work was to study the $(Mn, Zr)O_2$ catalyst state under redox conditions of propane oxidation. The catalyst state was investigated by powder X-ray diffraction (XRD) directly under catalytic oxidation conditions simultaneously with the detection of reaction products by a quadrupole mass spectrometer or operando.

EXPERIMENTAL

Synthesis. Catalysts with the ratio Mn/Zr = 3/7 were prepared by precipitating hydroxides from a combined solution of $ZrO(NO_3)_2$ and $Mn(NO_3)_2$ salts by a gradual addition of NH_3(aq) to it with constant stirring up to pH 10. The obtained precipitate was filtered off, washed with water to pH 6, dried at 120 °C, and then calcined at a given temperature for 4 h. The treatment temperature was varied from 400 °C to 800 °C. Catalysts were designated as Mn–Zr-*T*, where *T* is the calcination temperature. The Mn content in the catalyst is governed by that, according to the reported data, a homogeneous solid solution is formed at the ratio Mn/Zr = 3/7 [12].

Ex situ and operando powder XRD. XRD patterns of initial samples were measured on a Bruker D8 Advance (Germany) diffractometer in the 2θ range from 20° to 90° with a step of 0.05° and a point acquisition time of 5 s. CuK_α radiation with a nickel filter was used (λ = 1.5418 Å). The operando analysis was carried out on a precision diffractometry station installed on the sixth channel of the VEPP-3 storage ring (Siberian Synchrotron Radiation Center, Novosibirsk, Russia). The X-ray diffractometer on the station consisted of a monochromator, a collimation system, and a linear OD-3M detector [14]. The working wavelength (λ = 1.6467 Å) was set by a single reflection from the Ge(111) monochromator crystal. The diffractometer was equipped with a high-temperature XRK-900 (Anton Paar, Austria) reactor chamber. To control the gas medium we employed a quadrupole mass spectrometer (SRS UGA100, USA). The heating was conducted with a constant rate of 10°/min; the gas mixture supply rate was 100 mL/min. For the phase analysis we used ICDD PDF-2 [15]. The quatitative phase analysis and the lattice parameter refinement were made by the Rietveld method using the MAUD program [16].

Catalytic tests of the samples in the C_3H_8 oxidation reaction were performed on a flow-type apparatus in a glass reactor of 300 mm × ∅ 15 mm. The initial gas mixture was: 2% C_3H_8, 98% air, and its total consumption was 157 mL/min. The reaction mixture was chromatographically analyzed before and after the reactor with separating the mixture on a capillary column (stationary phase - SiO_2, 30 m × 0.32 mm). The unreacted amount of C_3H_8 was determined by the flame ionization detector. Before the catalytic tests the samples were pressed in pellets followed by grinding and fractioning. For the catalytic tests a 0.4-0.8 mm fraction was used. The sample weight was 0.5 g; it was mixed with quartz of the same fraction composition. The temperature in the catalyst layer was controlled and regulated by a chromel-alumel thermocouple connected with a Wart thermostat.

The reaction rate (activity) A was calculated from the degrees of C_3H_8 conversion with regard to thecatalyst weight

$$X_{C3H8} = (P_0 - P)/P_0,$$

$$A = X_{C3H8} \times V_{C3H8}/m_{кат}\ (cm^3/g{\cdot}s),$$

where P_0, P are the areas of C_3H_8 peaks before and after the reaction; V_{C3H8} (bulk rate of the propane flow) = V*α, V is the total flow rate of 157 mL/min; α is the propane concentration of 2%.

RESULTS AND DISCUSSION

Catalytic activity in propane oxidation. Fig. 1 demonstrates the activity (propane oxidation reaction rate) calculated at 250 °C for the catalysts under study. With increasing synthesis temperature from 400 °C to 650 °C an increase in the activity is observed from $8.30{\cdot}10^{-3}$ $cm^3(C_3H_8)/(g{\cdot}s)$ to $11.2{\cdot}10^{-3}$ $cm^3(C_3H_8)/(g{\cdot}s)$. A further increase in the calcination temperature leads to a decrease in the catalytic activity: e.g., for the Mn–Zr-800 catalyst the activity is $7.87{\cdot}10^{-3}$ $cm^3(C_3H_8)/(g{\cdot}s)$. Similar dependences were observed previously in the CO oxidation reaction for the MnO_x–ZrO_2 catalyst with the cation ratio Mn/Zr = 0.12/0.92; the maximum catalytic activity was detected at the calcination temperature of 650-700 °C and was due to the formation of the solid solution (Mn, Zr)O_2 [17]. Thus, the Mn–Zr-650 catalyst is characterized by the highest activity, and it was used in further studies.

Characterization of the initial state. The XRD pattern of the Mn–Zr-650 catalyst in the initial state exhibits intense peaks at 2θ = 30.5°, 35.4°, 50.9°, 60.6°, 63.6°, 74.9°, 83.0°, 85.7°, which correspond to 111, 200, 220, 311, 222, 400, 331,

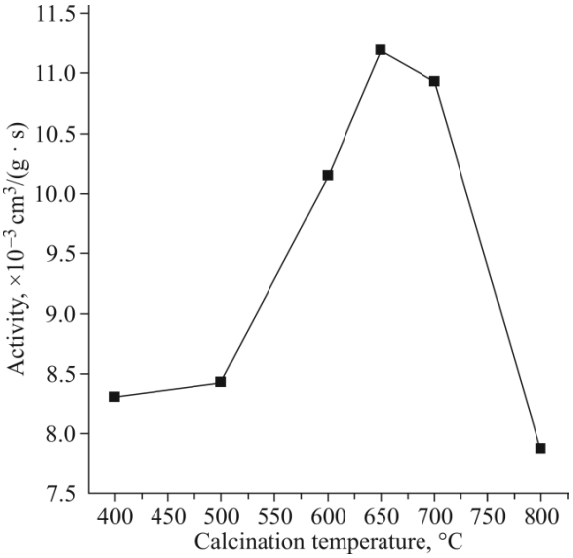

Fig. 1. Catalytic activity of Mn–Zr catalysts at the reaction temperature of 250 °C depending on the calcination temperature.

420 reflections of (Mn, Zr)O_2 space group *Fm*3*m* (PDF No. 77-2157) (Fig. 2). Moreover, there are peaks of manganese oxides at 2°θ = 32.9°, 55.1°, which correspond to 222, 400 reflections of Mn_2O_3 (PDF No. 41-1442). The lattice parameter of the phase based on zirconia is 5.052(2) Å for Mn–Zr-650, which is less than 5.128 Å for pure oxygen-deficient zirconia of the $ZrO_{1.7}$ cubic modification of the space group *Fm*3*m* (PDF No. 49-1642). Since the manganese cation has a smaller ionic radius than zirconium (Zr^{4+} = 0.72 Å (VI), Mn^{4+} = 0.53 Å (VI) [18]), a decrease in the lattice parameter indicates the formation of the (Mn, Zr)O_2 solid solution. According to the dependence of the lattice parameter on the manganese concentration in (Mn, Zr)O_2 solid solutions reported in [12], the obtained solid solution corresponds to the value of 25(3) at% Mn. Average CSR dimensions of (Mn, Zr)O_2 were 11 nm, Mn_2O_3 > 100 nm. In the case of the (Mn, Zr)O_2 solid solution, some underestimation of the CSR value cannot be excluded because of a possible deviation of the local composition from the average one and the occurrence of microdistortions.

Operando XRD studies of the propane oxidation reaction. To determine the phase composition and activity of the catalyst under conditions of the propane oxidation reaction we performed the operando XRD and mass spectrometric analysis of the Mn–Zr-650 catalyst. During the experiments the sample was heated to 550 °C with a rate of 5 °C/min. The reaction mixture of the composition 1%C_3H_8/6%O_2/He was used in the work, i.e. the ratio C_3H_8/O_2 = 1/6 at which the reaction mixture contained a small excess of oxygen relative to the stoichiometry of the oxidation reaction ($C_3H_8 + 5O_2 \rightarrow 3CO_2 + 4H_2O$). Fig. 3*a* depicts the XRD patterns recorded during heating of the reaction medium. It is seen that there are no changes in the phase composition. In the entire temperature range there are reflections of the (Mn, Zr)O_2 solid solution and Mn_2O_3 oxide. However, with increasing temperature the lattice parameter of the (Mn, Zr)O_2 solid solution increases to 5.065 Å (Fig. 3*c*). The active component of MnO_x–ZrO_2 catalysts in hydrocarbon and CO oxidation reactions has been discussed. There is no consensus on the nature of the catalytic activity of MnO_x–ZrO_2 in the publications. According to the first concept, Mn cations can enter into the ZrO_2 structure, forming a (Mn, Zr)O_2 solid solution [19-21] in which anionic vacancies are formed, lattice oxygen acquires a high mobility, and consequently, a high reactivity. The alternative assumption is that mobile oxygen of dispersed MnO_x not contained in the composition of the solid solution is active in the oxidation reactions [22]. Here it is worth noting that a change in the lattice parameter of the solid solution is a sensitive characteristic responsible for the chemical composition, the occurrence of defects, and the charge state of cations in the solid solution.

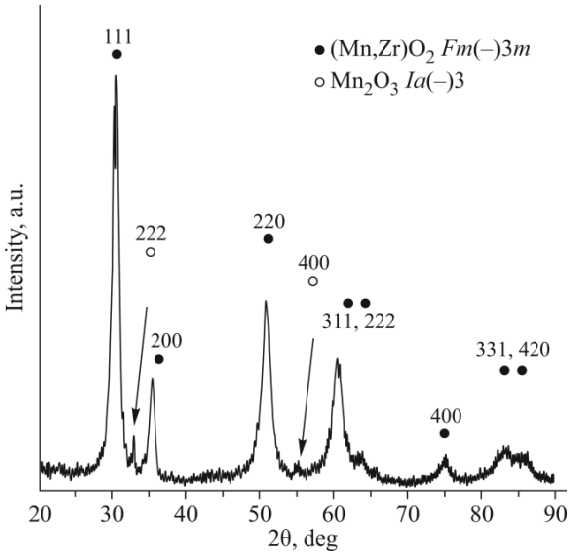

Fig. 2. XRD pattern of the Mn–Zr-650 catalyst. Radiation wavelength of 1.5418 Å.

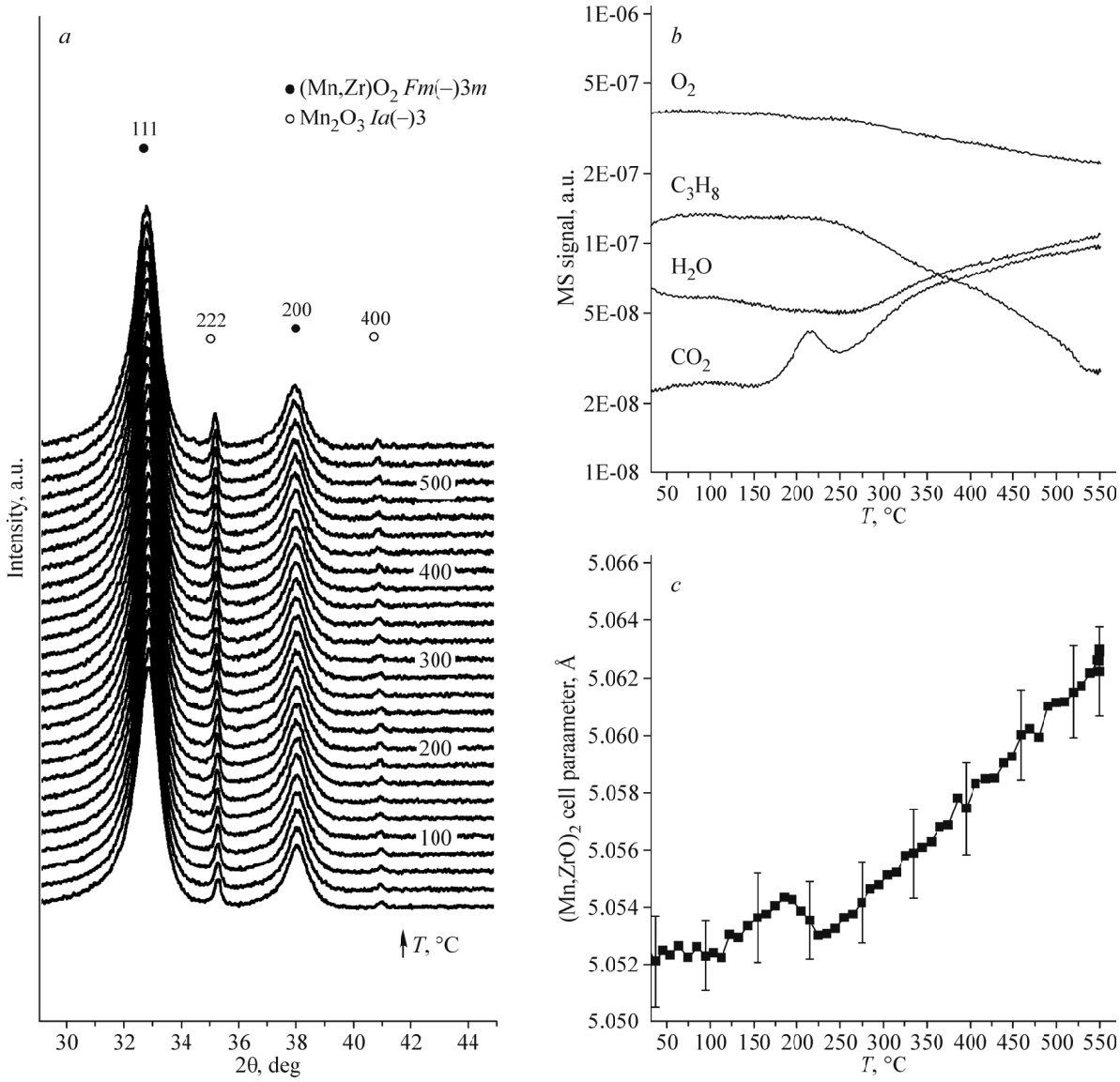

Fig. 3. XRD patterns of Mn–Zr-650 recorded upon heating from 30 °C to 550 °C with a rate of 5 deg/min in the 1%C_3H_8/6%O_2/He reaction medium; 1.6467 Å wavelength (*a*) and mass spectrometry data obtained simultaneously (*b*); change in the lattice parameter of (Mn,Zr)O_2 with temperature (*c*).

A change in the gas phase state is illustrated in Fig. 3*b*. According to the mass spectrometry data, starting from 230 °C, a decrease in the propane and O_2 signal is observed along with an increase in the CO_2 curve, which indicates that the propane oxidation reaction proceeds on the catalyst. An insignificant peak on the CO_2 signal curve in the temperature range of 150-230 °C is likely to be due to a release of adsorbed gas.

In order to establish the nature of changes in the lattice parameter of the solid solution, additional experiments were carried out: the heating in oxidizing (20%O_2/He) and reducing (5.3%C_3H_8/He) media. In the oxygen-containing atmosphere no changes take place in the XRD patterns, there are (Mn, Zr)O_2 and Mn_2O_3 reflections (the figure is not given), and the lattice parameter increases to 5.062(1) Å upon heating. Under heating condition in the propane medium, the phase composition of the catalyst changes (Fig. 4*a*, *c*). At 420 °C the reflections of Mn_2O_3 oxide (2θ = 35.1°, 40.8°, *hkl* = 222, 004) disappear and new low-intensity peaks appear at 2θ = 34.6°, 38.5° which correspond to 103, 211 reflections of Mn_3O_4 oxide (PDF No. 24-734). At T = 450 °C, Mn_3O_4 oxide completely transforms into MnO, which is evidenced by reflections at 2θ = 37.2°, 43.2° (*hkl* = 111, 200) (PDF No. 7-230). From Fig. 4*c* it is seen that after reduction the content of the solid

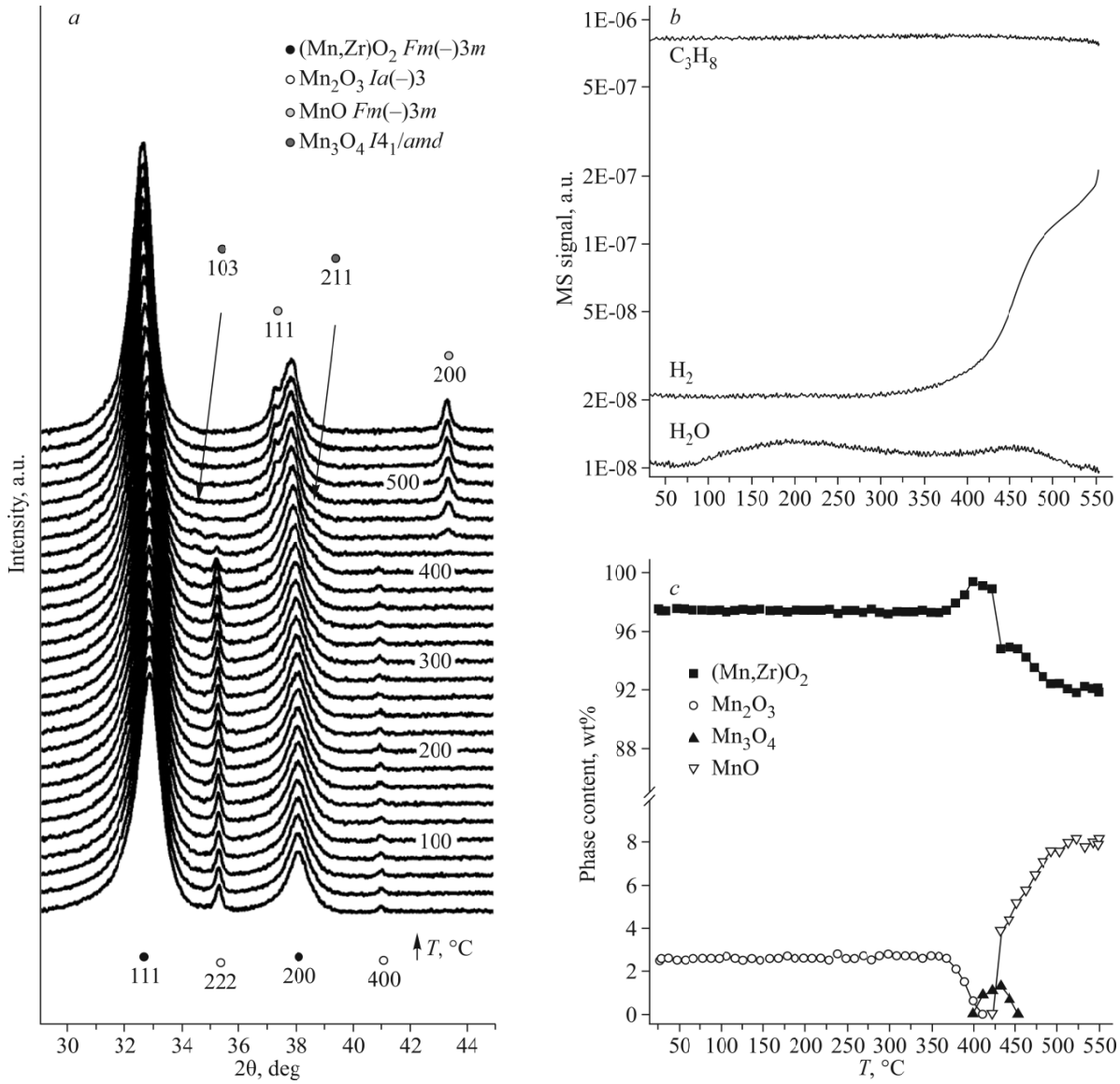

Fig. 4. XRD patterns of Mn–Zr-650 recorded upon heating from 30 °C to 550 °C with a rate of 5 deg/min in 5.3%C_3H_8/He, 1.6467 Å wavelength (*a*) and mass spectrometry data obtained simultaneously (*b*); change in the phase composition with temperature; in the Rietveld refinement of the XRD patterns the $Mn_{0.3}Zr_{0.7}O_2$ oxide model with a fixed cationic and anionic composition was used (*c*).

solution decreases from 97 wt% to 92 wt%, the weight fraction of manganese in the composition of simple oxides increases from 2.7 wt% (Mn_2O_3) (corresponds to 1.9 wt% Mn) to 8.2 wt% (MnO) (corresponds to 6.4 wt% Mn) during reduction, which in turn indicates the release of manganese from the composition of the solid solution. To simplify the quantitative estimation of contained phases (Fig. 4*c*) in the Rietveld refinement we used the solid solution with a fixed ratio of cations: $Mn_{0.3}Zr_{0.7}O_2$. On the other hand, it is assumed that the composition of mixed oxide changes during reduction, therefore, we additionally estimated the content of manganese cations in the solid solution. To this end, the amount of manganese in the solid solution was parametrically related to the refined value of the weight content of the manganese oxide phase (Mn_2O_3 or Mn_3O_4). The correlation coefficient was found through the theoretical calculation density and the molar weight of the respective phase. Here the following assumptions were used: for the solid solution the total cation site occupancy was 1, the oxygen site occupancy was calculated from the electroneutrality balance with regard to Mn^{3+} and Zr^{4+} oxidation states, the other phases had the stoichiometric composition. Since the correlation coefficient also depends on the composition of the solid solution, it was found iteratively from the previous calculation cycle, starting from the $Mn_{0.3}Zr_{0.7}O_2$ model. For a three-

phase system such a calculation is impossible in MAUD, therefore the refinement was made for two extreme cases: the initial state and at 550 °C. Final results (Fig. 5) show that the initial catalyst contains 2.2 wt.% for Mn_2O_3 and 97.8 wt.% for $Mn_{0.28}Zr_{0.72}O_{1.86}$; after reduction at 550 °C - 8.1 wt% for MnO and 91.9 wt% for $Mn_{0.24}Zr_{0.76}O_{1.88}$. The data obtained also testify in favor of the removal of manganese cations from the composition of the solid solution, as well as the previous estimates based on the calculation with the fixed composition of $Mn_{0.3}Zr_{0.7}O_2$ oxide.

The comparison of lattice parameters of the solid solution in different atmospheres is illustrated Fig. 6. It is seen that temperature dependences of parameters coincide under the reaction conditions and in oxygen. This indicates that the catalyst structure does not change under propane oxidation conditions. It is considered that for manganese-containing oxides the oxidation reaction proceeds by the Mars–Van Krevelen mechanism, the reagent is oxidized by lattice oxygen from the structure of mixed oxide with the formation of reaction products, the oxygen vacancy is “healed” with oxygen from the gas phase [23]. In our case, XRD does not detect changes in the oxide structure, which seems to be due to exclusively surface changes in the catalyst structure. Similar effects were also observed for manganese-containing catalysts in the CO oxidation reaction: when the substrate (CO) interacts with oxygen from the gas phase on the catalyst surface under the conditions of an oxygen excess in the gas phase, no changes in the catalyst structure are detected [13] unlike copper-containing catalysts in which partial reduction of copper cations is observed under the reaction conditions [24].

In the propane medium (without oxygen), manganese cations are reduced. Under these conditions the lattice parameter substantially exceeds the values for the oxygen-containing medium. At first, ero insignificant changes are observed in the temperature range of 25-180 °C, then there is an abrupt increase from 5.052 Å to 5.081 Å at 180-460 °C, after which the parameter slowly increases to 5.085 Å at 460-550 °C. An increase in the lattice parameter may be associated with both reduction of Mn cations in the solid solution bulk (since the Mn^{2+} (VI) cationic radius is 0.67 Å larger than that of Mn^{3+} (VI) 0.58 Å, Mn^{4+} (VI) 0.53 Å) [18] and decomposition of the solid solution with the formation of additional phases of manganese oxides. When manganese is released from the solid solution, the lattice parameter must increase because of the difference between Mn and Zr ionic radii. The fact that there is an increase in the weight content of manganese in the composition of simple oxides after treatment (Fig. 4*c*) and the estimation of the solid solution composition (Fig. 5) testifies in favor of the

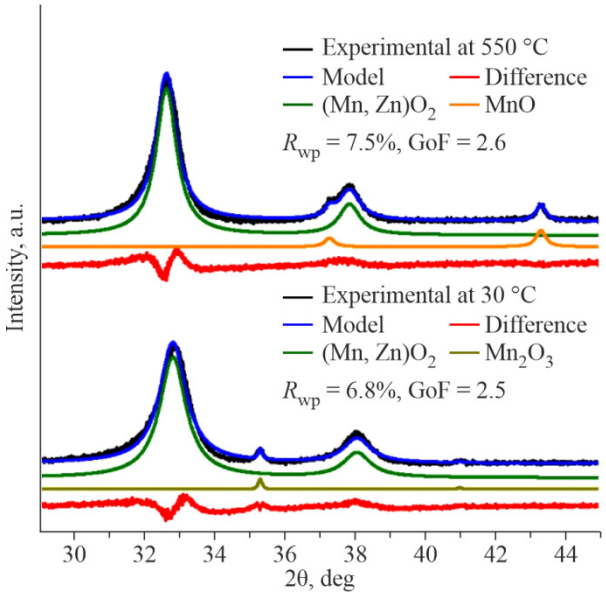

Fig. 5. Full-profile refinement of the XRD patterns of Mn–Zr-650 obtained for the initial state of the catalyst (*b*) and at 550 °C in the 5.3% C_3H_8/He medium (*a*).

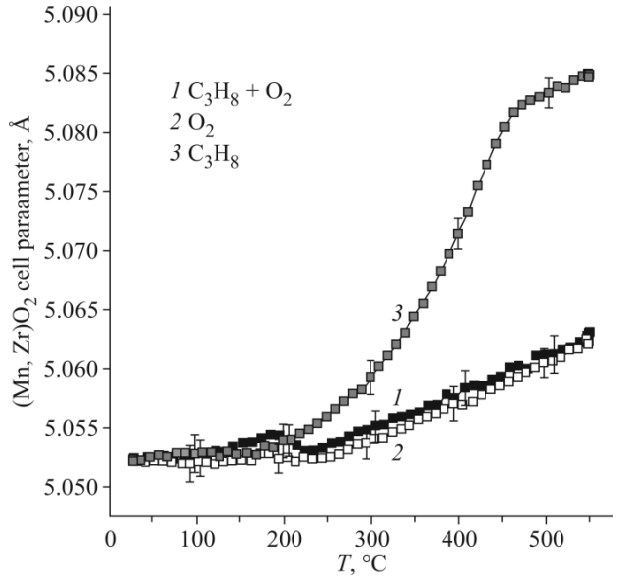

Fig. 6. Change in the lattice parameter of $(Mn,Zr)O_2$ with temperature under the reaction conditions $1\%C_3H_8/6\%O_2/He$ (*1*), $20\%O_2/He$ (*2*), $5.3\%C_3H_8/He$ (*3*).

latter assumption. According to the mass spectrometry data, at $T = 420$-550 °C an H_2 signal appears and the propane signal decreases (Fig. 4*b*). The observed phenomenon may be explained by the occurrence of the catalytic propane dehydrogenation reaction $C_3H_8 \rightarrow C_3H_6 + H_2$. It is known that ZrO_2 is the catalyst of this reaction where active centers are coordinatively unsaturated Zr atoms forming during the removal of oxygen from the oxide structure [25-27]. Manganese cations can enhance this effect due to the formation of additional oxygen vacancies. Hydrogen released during the reaction can also be involved in catalyst reduction.

CONCLUSIONS

In the work, we took advantages of operando XRD to analyze the Mn–Zr oxide catalyst under propane oxidation reaction conditions. The initial catalyst consisted of the $(Mn, Zr)O_2$ solid solution and Mn_2O_3 oxide. The structural features of the catalyst were investigated during heating in propane, oxygen and propane oxidation reaction conditions at the propane:oxygen ratio of 1:6. In pure propane, the dehydrogenation reaction takes place on the catalyst, which is accompanied by the formation of propylene and hydrogen. At the same time, the catalyst structure changes, Mn cations are reduced in both $(Mn, Zr)O_2$ solid solution bulk and composition of crystalline oxides in the order: $Mn_2O_3 \rightarrow Mn_3O_4 \rightarrow MnO$. Under catalytic reaction conditions of propane oxidation and in pure oxygen, the phase composition of the catalyst remains unchanged.

FUNDING

The work was supported by RFBR and the Novosibirsk Oblast' within scientific project No. 19-43-543012.

ACKNOWLEDGMENTS

For the in situ XRD analysis the facilities of the Siberian Synchrotron Radiation Center based on VEPP-4-VEPP-2000 complex in the Budker Institute of Nuclear Physics, Siberian Branch, Russian Academy of Sciences.

CONFLICT OF INTERESTS

The authors declare that they have no conflicts of interests.

REFERENCES

1. H. Xu, N. Yan, Z. Qu, W. Liu, J. Mei, W. Huang, and S. Zhao. *Environ*. *Sci*. *Technol*., **2017**, *51*, 8879. https://doi.org/10.1021/acs.est.6b06079
2. C. Cellier, V. Ruaux, C. Lahousse, P. Grange, and E. M. Gaigneaux. *Catal*. *Today*, **2006**, *117*, 350. https://doi.org/10.1016/j.cattod.2006.05.033
3. P. G. Tsyrul′nikov, V. S. Sal′nikov, V. A. Drozdov, S. A. Stuken, A. V. Bubnov, E. I. Grigorov, A. V. Kalinkin, and V. I. Zaikovskii. *Kinet*. *Catal*., **1991**, *32*, 387.
4. R. Craciun, B. Nentwick, K. Hadjiivanov, and H. Knözinger. *Appl*. *Catal*., *A*, **2003**, *243*, 67. https://doi.org/10.1016/S0926-860X(02)00538-0
5. E. R. Stobbe, B. A. De Boer, and J. W. Geus. *Catal*. *Today*, **1999**, *47*, 161. https://doi.org/10.1016/S0920-5861(98)00296-X
6. J. Pike, J. Hanson, L. Zhang, and S.-W. Chan. *Chem*. *Mater*., **2007**, *19*, 5609. https://doi.org/10.1021/cm071704b
7. O. A. Bulavchenko, O. S. Venediktova, T. N. Afonasenko, P. G. Tsyrul′nikov, A. A. Saraev, V. V. Kaichev, and S. V. Tsybulya. *RSC Adv*, **2018**, *8*, 11598. https://doi.org/10.1039/c7ra11557a
8. O. A. Bulavchenko, E. Y. Gerasimov, and T. N. Afonasenko. *Dalton Trans*., **2018**, *47*, 17153. https://doi.org/10.1039/c8dt04137g
9. O. A. Bulavchenko, T. N. Afonasenko, S. S. Sigaeva, A. V. Ivanchikova, A. A. Saraev, E. Y. Gerasimov, V. V. Kaichev, and S. V. Tsybulya. *Top*. *Catal*., **2020**, *63*, 75. https://doi.org/10.1007/s11244-020-01230-1
10. O. A. Bulavchenko, T. N. Afonasenko, A. V. Ivanchikova, V. Y. Murzin, A. M. Kremneva, A. A. Saraev, V. V. Kaichev, and S. V. Tsybulya. *Inorg*. *Chem*., **2021**, *60*, 16518. https://doi.org/10.1021/acs.inorgchem.1c02379
11. O. S. Venediktova, O. A. Bulavchenko, T. N. Afonasenko, P. G. Tsyrul′nikov, Z. S. Vinokurov, Y. A. Chesalov, and S. V. Tsybulya. *J*. *Alloys Compd*., **2017**, *725*, 496. https://doi.org/10.1016/j.jallcom.2017.07.175
12. O. A. Bulavchenko, Z. S. Vinokurov, T. N. Afonasenko, P. G. Tsyrul′nikov, S. V. Tsybulya, A. A. Saraev, and V. V. Kaichev. *Dalton Trans*., **2015**, *44*, 15499. https://doi.org/10.1039/c5dt01440a
13. O. A. Bulavchenko, Z. S. Vinokurov, T. N. Afonasenko, and S. V. Tsybulya. *Mater*. *Lett*., **2020**, *258*, 126768. https://doi.org/10.1016/j.matlet.2019.126768
14. O. V. Evdokov, V. M. Titov, B. P. Tolochko, and M. R. Sharafutdinov. *Nucl*. *Instrum*. *Methods Phys*. *Res*., *Sect*. *A*, **2009**, *603*, 194. https://doi.org/10.1016/j.nima.2009.03.001
15. S. Gates-Rector and T. Blanton. *Powder Diffr*., **2019**, *34*, 352. https://doi.org/10.1017/S0885715619000812
16. L. Lutterotti. *Nucl*. *Instrum*. *Methods Phys*. *Res*., *Sect*. *B*, **2010**, *268*, 334. https://doi.org/10.1016/j.nimb.2009.09.053
17. T. N. Afonasenko, O. A. Bulavchenko, T. I. Gulyaeva, S. V. Tsybulya, and P. G. Tsyrul′nikov. *Kinet*. *Catal*., **2018**, *59*, 104. https://doi.org/10.1134/S0023158418010019
18. R. D. Shannon. *Acta Crystallogr*., *Sect*. *A*, **1976**, *32*, 751. https://doi.org/10.1107/S0567739476001551
19. F. Kapteijn, L. Singoredjo, A. Andreini, and J. A. Moulijn. *Appl*. *Catal*., *B*, **1994**, *3*, 173. https://doi.org/10.1016/0926-3373(93)E0034-9
20. V. R. Choudhary, S. Banerjee, and S. G. Pataskar. *Proc*. *Indian Acad*. *Sci*., **2003**, *115*, 287. https://doi.org/10.1007/BF02704220
21. K. Zeng, X. Li, C. Wang, Z. Wang, P. Guo, J. Yu, C. Zhang, and X. S. Zhao. *J*. *Colloid Interface Sci*., **2020**, *572*, 281. https://doi.org/10.1016/j.jcis.2020.03.093

22. J. I. Gutiérrez-Ortiz, B. de Rivas, R. López-Fonseca, S. Martín, and J. R. González-Velasco. *Chemosphere*, **2007**, *68*, 1004. https://doi.org/10.1016/j.chemosphere.2007.02.025
23. K. Ramesh, L. Chen, F. Chen, Y. Liu, Z. Wang, and Y.-F. Han. *Catal*. *Today*, **2008**, *131*, 477. https://doi.org/10.1016/j.cattod.2007.10.061
24. A. A. Saraev, A. M. Tsapina, A. V. Fedorov, A. L. Trigub, O. A. Bulavchenko, Z. S. Vinokurov, Y. V. Zubavichus, and V. V. Kaichev. *Radiat*. *Phys*. *Chem*., **2020**, *175*, 108071. https://doi.org/10.1016/j.radphyschem.2018.11.025
25. Y. Zhang, Y. Zhao, T. Otroshchenko, S. Han, H. Lund, U. Rodemerck, D. Linke, H. Jiao, G. Jiang, and E. V. Kondratenko. *J*. *Catal*., **2019**, *371*, 313. https://doi.org/10.1016/j.jcat.2019.02.012
26. T. Otroshchenko, V. A. Kondratenko, U. Rodemerck, D. Linke, and E. V. Kondratenko. *J*. *Catal*., **2017**, *348*, 282. https://doi.org/10.1016/j.jcat.2017.02.016
27. T. Otroshchenko, O. Bulavchenko, H. V. Thanh, J. Rabeah, U. Bentrup, A. Matvienko, U. Rodemerck, B. Paul, R. Kraehnert, D. Linke, and E. V. Kondratenko. *Appl*. *Catal*., *A*, **2019**, *585*, 1. https://doi.org/10.1016/j.apcata.2019.117189